

# Statistics of Broadband Echoes: Application to Acoustic Estimates of Numerical Density of Fish

Wu-Jung Lee, *Member, IEEE*, and Timothy K. Stanton

**Abstract**—A general numerical model has been developed to predict the probability density function (pdf) of the magnitudes of complex pulse-compressed broadband echoes (broadband echo pdf) due to arbitrary aggregations of scatterers that are detected with a single-beam echosounder. The model is based on physics principles and rigorously accounts for the broadband frequency-dependent characteristics of the system, signal, scatterers, and the beampattern modulation effects of the sonar/radar transceiver. A key aspect to modeling the statistics of broadband echoes is accounting for the scenarios where the pulse-compressed echoes may only partially overlap. The echo statistics under those conditions will be significantly different than those associated with a narrowband system with the same center frequency but whose echoes will completely overlap given the same density of scatterers. As a result, pulse-compressed broadband echoes will generally deviate more from the Rayleigh distribution (i.e., be more “heavy-tailed”) than narrowband echoes—a feature that is critical to analyzing real-world data. As in the case of narrowband signals, the shape of the broadband echo pdf is shown to vary from strongly non-Rayleigh to Rayleigh as the number of dominant scatterers in the beam increases. The model is applied to sonar in the ocean in which the numerical density of fish is inferred using broadband echoes (30–70 kHz). The results are compared with those from conventional echo energy methods. As with narrowband systems, statistics of broadband echoes can be used to estimate the numerical density of scatterers without the need for absolute calibration of the system.

**Index Terms**—Beampattern, broadband, echo statistics, non-Rayleigh, numerical density of scatterers.

## I. INTRODUCTION

THE ability to characterize and infer the sources of scattering from echoes is of crucial importance for remote sensing applications, such as with sonar and radar systems. As the sonar/radar beam scans across a volume or area of interest, the echoes fluctuate from ping to ping as a result of the variation of scatterer composition, orientation, location within the beam,

and numerical density, all of which are random variables [1], [2]. The statistics of echoes, such as the shape of the probability density function (pdf) of the magnitudes of complex echoes (hereafter referred to as “echo pdf”), provide an avenue for echo characterization and discrimination. Different from the conventional echo energy techniques where mean echo spectra are utilized, echo statistics methods associate fluctuations of the echoes with the scattering properties of the same scatterer or the same set of scatterers in an empirical or physics-based manner [1]–[4]. Statistical characterization of echoes is widely used in many remote sensing fields, including electromagnetic scattering from the sea surface or terrestrial vegetation using radar, and acoustic scattering from seafloor features and marine organisms using sonar [1], [2]. It also has an advantage over the echo energy methods in applications such as estimating numerical density of scatterers, as absolute calibration of the system is not required for echo statistics analysis [5], [6].

The statistics of echoes depend strongly on the degree to which the echoes from individual scatterers overlap and the statistical features of echoes from the individuals. When the echoes are formed by coherent summation of a large number of random scatterers, the echo pdf converges asymptotically to the Rayleigh distribution [7]. This is a direct consequence of the central limit theorem, in which both the real (in-phase) and imaginary (quadrature) components of the overlapping echoes are Gaussian distributed. When any one of the above conditions is not satisfied, non-Rayleigh-distributed echoes with heavy tails can occur. Here, the “tail” is defined as the portion of the pdf where values of the echo amplitude are relatively high and the probability densities are relatively low. It is the shape of the echo pdf, particularly at the tail, and the degree to which an echo pdf deviates from the Rayleigh distribution that give the discriminative features for echo statistics analysis [8].

The development of statistical models for non-Rayleigh echo pdfs has been one of the major focuses in underwater sonar research in the past decade [1]. Most of these studies took a data-driven approach to determine the best statistical representation of echoes by fitting echo observations to generic probabilistic distributions or their mixture (e.g., [9] and [10]). However, these models were derived empirically without explicit connections between model parameters and the sources of scattering. Therefore, the models are not predictive, and their application is often limited to data collected using similar systems in specific geographical locations. To overcome these problems, a number of other studies took a physics-based approach to derive theoretical echo statistics models by rigorously considering the various components in the acoustic scattering processes, including characteristics of the system, signal, and scat-

Manuscript received February 01, 2015; revised July 18, 2015 and August 10, 2015; accepted August 29, 2015. Date of publication December 01, 2015; date of current version July 12, 2016. This work was supported by two National Oceanographic Partnership Program (NOPP) projects through the U.S. Office of Naval Research (ONR), as well as the Academic Programs Office at the Woods Hole Oceanographic Institution.

**Associate Editor:** N. Chotiros.

W.-J. Lee was with the Department of Applied Ocean Physics and Engineering, Woods Hole Oceanographic Institution, Woods Hole, MA 02543-1053 USA. She is now with the Department of Psychological and Brain Sciences, Johns Hopkins University, Baltimore, MD 21218-2686 USA (e-mail: wjlee@jhu.edu).

T. K. Stanton is with the Department of Applied Ocean Physics and Engineering, Woods Hole Oceanographic Institution, Woods Hole, MA 02543-1053 USA (e-mail: tstanton@whoi.edu).

Digital Object Identifier 10.1109/JOE.2015.2476619

tering sources (e.g., [4] and [11]). By establishing the connections among model parameters, echo pdf features, and dominant sources of scattering, these models can be used as inference tools to characterize echoes from scattering sources in a direct-path geometry [12]–[15] or under the influence of a waveguide with reflecting boundaries [16]. In addition, these models can be used to predict the performance of sonar/radar systems over a wide range of conditions where echoes from targets of interest need to be discriminated from unwanted echoes, such as those due to clutter [6], [10].

In the field of acoustical oceanography, recent advancements in high-frequency broadband echosounders [17]–[19] have made statistical methods even more applicable to study the echoes from aggregations of marine organisms. Specifically, the temporal resolution of broadband echoes is substantially improved through pulse compression [20], often from tens of centimeters to only a few centimeters [19]. The improved temporal resolution reduced the extent to which echoes from multiple scatterers overlap in typical scenarios where a large number of marine organisms are insonified by a single (unprocessed) sonar ping. This leads to a higher probability of observing non-Rayleigh features that are critical for echo statistics analysis. However, current echo statistics models are generally incompatible with the newly available broadband echo data due to the assumption that the signals are continuous wave (CW) [6], [14]–[16].

There are several outstanding challenges in modeling the statistics of broadband echo envelopes. Broadband pulse-compressed echoes are temporally localized and cannot be represented using random phasors of infinite time span as has been done under the CW assumption. Instead, the broadband echo pdfs are formed by envelope samples of partially overlapping echo pulses with varying shapes. The fact that individual broadband echoes only partially overlap is a key element in modeling the statistics as broadband echoes tend toward being non-Rayleigh under the same conditions where a narrowband signal (overlapping echoes) tends to be Rayleigh. The shapes of the pulses are jointly determined by the spectral content of the signal and the frequency response of the system and scatterers. They are also influenced heavily by the beam pattern modulation determined by the random locations of the scatterers in the beam of the sonar/radar receiver, which is critical in modeling the non-Rayleigh features in the echo pdf [14], [21]. These considerations make it difficult to formulate into a closed-form solution the exact analytical description of broadband echo pdfs over the entire amplitude range.

A Monte Carlo numerical model is developed in this study to describe the distribution of the magnitudes of pulse-compressed broadband echoes (i.e., “broadband echo pdf”) from random scatterers. This model is developed based on a physics-based approach and rigorously accounts for the influence of frequency-dependent characteristics of the system, signal, scatterer, and the beam pattern modulation effects of the sonar/radar receiver. The model assumes a geometry involving direct paths between the echosounder and the scatterers without interference from boundaries. Properties of the broadband echo pdf model are investigated using parameters consistent with the broadband

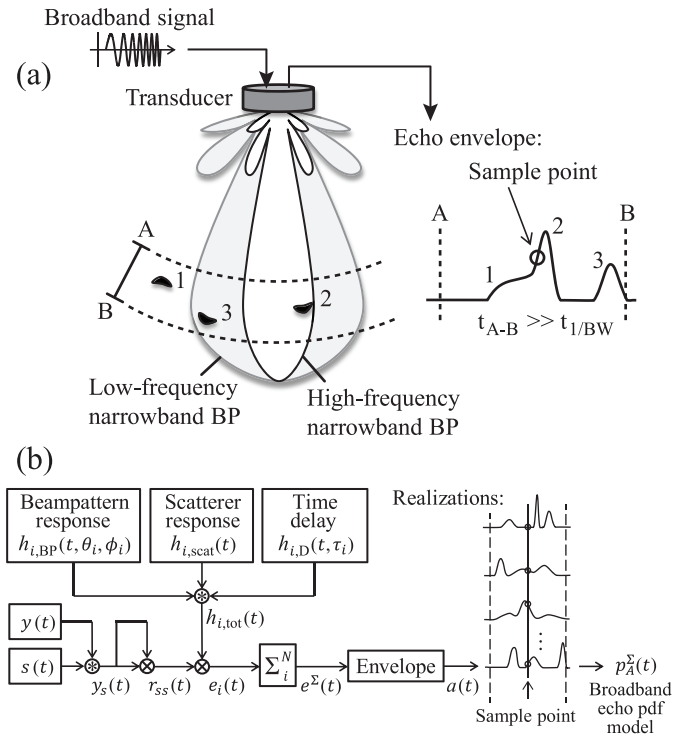


Fig. 1. (a) Schematic showing one realization of the numerical model. The sample point is chosen to be fixed at the midpoint of the analysis gate  $\overline{AB}$  ( $= L_g$  in text), which corresponds to a hemispherical shell in three dimensions. The frequency-dependent property of beam pattern modulation is illustrated using a low-frequency and a high-frequency narrowband beam pattern (BP) produced by a circular aperture. Echoes are modulated according to the locations of scatterers in the beam. In contrast to the other two scatterers, scatterer #2 is located within the mainlobes of both the low- and high-frequency beams and results in a sharper echo (see Section II-B). (b) Block diagram of the procedure of numerical simulation. The ensemble of samples collected from multiple independent realizations is used for generating the broadband echo pdf model.

frequency-dependent characteristics of a commercially available high-frequency single-beam acoustic echosounder. Such a system is typically found in the acoustic scattering studies of marine organisms [Fig. 1(a)]. Comparisons are also made between predicted broadband echo pdfs and predicted narrowband echo pdfs whose frequency is at the center of the frequency spectrum of the broadband signal. The model is first applied over a range of conditions to two generic scatterers—one whose echoes without beam pattern effects are Rayleigh distributed (hereafter referred to as a “Rayleigh scatterer”) and the other a prolate spheroid whose echoes without beam pattern effects are non-Rayleigh. The model is then applied to estimate the numerical density of fish observed with sonar in the Gulf of Maine using a fish scattering model. Estimates of the numerical densities of fish using the broadband echo pdf model are compared with estimates given by echo energy methods which interpret volume backscattering strength ( $S_V$ ) using modeled target strength (TS). Limitations of the broadband echo pdf as a tool for echo analysis and potential errors associated with various model assumptions are discussed.

The paper is organized as follows. The numerical modeling framework for broadband echo pdfs and the results of model implementation for Rayleigh scatterers and prolate spheroids are presented in Section II. Details of the selection and processing

of sonar echo data from the ocean experiment are discussed in Section III. In Section IV, the numerical densities of fish are estimated using the broadband echo pdf model and two echo energy methods, and the results are compared. The summary and conclusion of this study are given in Section V.

## II. NUMERICAL SIMULATIONS OF BROADBAND ECHO PDFS

### A. Modeling Framework

The broadband echo pdf model in this study is developed in the time domain based on the temporally localized features of broadband echoes after pulse compression processing [Fig. 1(a)]. The model is obtained numerically by drawing samples from repeated independent realizations to form the probability distribution of broadband echo envelopes.

In contrast to the echoes of CW signals that are of infinite length, pulse-compressed broadband echoes are localized in time and will generally, at most, only partially overlap with one another. In the model setup, an analysis gate of length  $\tau$  is arbitrarily chosen to represent the temporal (and thus, spatial) span of the analysis window from which samples of the echo envelopes are taken. The volume included in this analysis gate is a hemispherical shell with thickness  $L_g$ , where  $L_g = c\tau/2$  and  $c$  is the speed in the medium of the sonar/radar signal. For each independent model realization, an echo time series is generated from a fixed number of randomly distributed scatterers ( $N$ ) enclosed in the hemispherical shell. The echo pdf is derived by an ensemble of samples taken from the envelope of the time series of repeated realizations. Note that the duration of the analysis gate  $\tau$  is much larger than the time associated with the range resolution which, after pulse compression, is approximately equal to the inverse of the bandwidth of the echoes [20] [Fig. 1(a)]. Thus, it is possible to have multiple nonoverlapping broadband echoes in the analysis gate.

The scatterers in the model are assumed to be randomly and uniformly distributed in the hemispherical shell. The physical location of each random scatterer is described by its temporal location in the analysis gate, which corresponds to the distance between the scatterer and the system, as well as its angular position with respect to the axis of the transducer aperture [Fig. 1(a)]. The random temporal location of each scatterer in the analysis gate is simulated by drawing a sample from a uniform distribution over a range of  $[0, \tau]$ . The random angular position of each scatterer is generated by calculating the polar and azimuthal angles of a point randomly and uniformly distributed within a hemispherical half-space.

A block diagram of the modeling procedure is illustrated [Fig. 1(b)]. Given a signal  $y(t)$  applied to the transducer and the impulse response of the sonar/radar system  $s(t)$  (which includes the frequency-dependent, two-way response of the transducer and both the transmit and receive circuits in the system), the replica of system-response-modified transmit signal  $y_s(t)$ , hereafter called “transmit replica,” is given by

$$y_s(t) = y(t) * s(t) \quad (1)$$

where “\*” denotes convolution.

The pulse-compressed echo from the  $i$ th scatterer is calculated by cross correlating the raw echo with the transmit replica and is given in a compact form as

$$e_i(t) = r_{ss}(t) \otimes h_{i,\text{tot}}(t) \quad (2)$$

where “ $\otimes$ ” denotes cross correlation,  $r_{ss}(t)$  is the autocorrelation function of the transmit replica

$$r_{ss}(t) = y_s(t) \otimes y_s(t) \quad (3)$$

and  $h_{i,\text{tot}}(t)$  is the composite impulse response of the  $i$ th scatterer which includes beampattern effects [20]. The composite impulse response can be expressed as

$$h_{i,\text{tot}}(t) = h_{i,\text{scat}}(t) * h_{i,D}(t, \tau_i) * h_{i,\text{BP}}(t, \theta_i, \phi_i) \quad (4)$$

where  $h_{i,\text{scat}}(t)$  is the impulse response of the scattering amplitude of the  $i$ th scatterer associated solely with its scattering properties,  $h_{i,D}(t, \tau_i) = \delta(t - \tau_i)$  represents the temporal location of the scatterer in the analysis gate, and  $h_{i,\text{BP}}(t, \theta_i, \phi_i)$  is the frequency-dependent weighting factor imposed by the transducer beampattern depending on the polar ( $\theta_i$ ) and azimuthal ( $\phi_i$ ) angles of the scatterer with respect to the axis of the transducer aperture. For the case of the circular aperture considered in this study, the beampattern response depends only on the polar angle, i.e.,  $h_{i,\text{BP}}(t, \theta_i, \phi_i) = h_{i,\text{BP}}(t, \theta_i)$ .

The pulse-compressed echo time series resulting from the contributions of  $N$  arbitrary scatterers is

$$e^\Sigma(t) = \sum_i^N e_i(t) \quad (5)$$

from which the envelope of the echoes  $a(t)$  ( $= |e^\Sigma(t)|$ ) is computed and a random sample from the envelope ( $a$ ) is drawn. For convenience in model implementation, the samples are drawn from a fixed location at the midpoint of the analysis gate [Fig. 1(b)]. Since the locations of the scatterers are random in the analysis gate, this is equivalent to drawing samples at random locations away from the edges of the analysis gate. Also, the analysis gate is chosen to be much smaller than the distance between the transducer and scatterers, resulting in approximately a constant range for the scatterers. Because of the negligible dependence of range in the scattering formulation, the range term is suppressed from the equation for simplicity. Other constant system factors are suppressed as well.

The kernel density method [22] is used to estimate a continuous and smooth broadband echo pdf  $p_A^\Sigma(a)$ . To avoid violating the condition that  $a \geq 0$  and to produce a smooth estimate of the tail of the pdf where the number of samples may be small, the envelope samples are log transformed before the kernel density estimation is performed. An inverse transform is used to obtain the final broadband echo pdf model in the linear domain. The kernel density estimation algorithm presented in [23] is used in this study.

Note that the term  $N$  in the model denotes the number of scatterers enclosed within the analysis gate over the entire half-space, which is normally much larger than the number of scatterers insonified/irradiated by only the mainlobe of the sonar/radar beam, which is typically narrow. The scatterers within

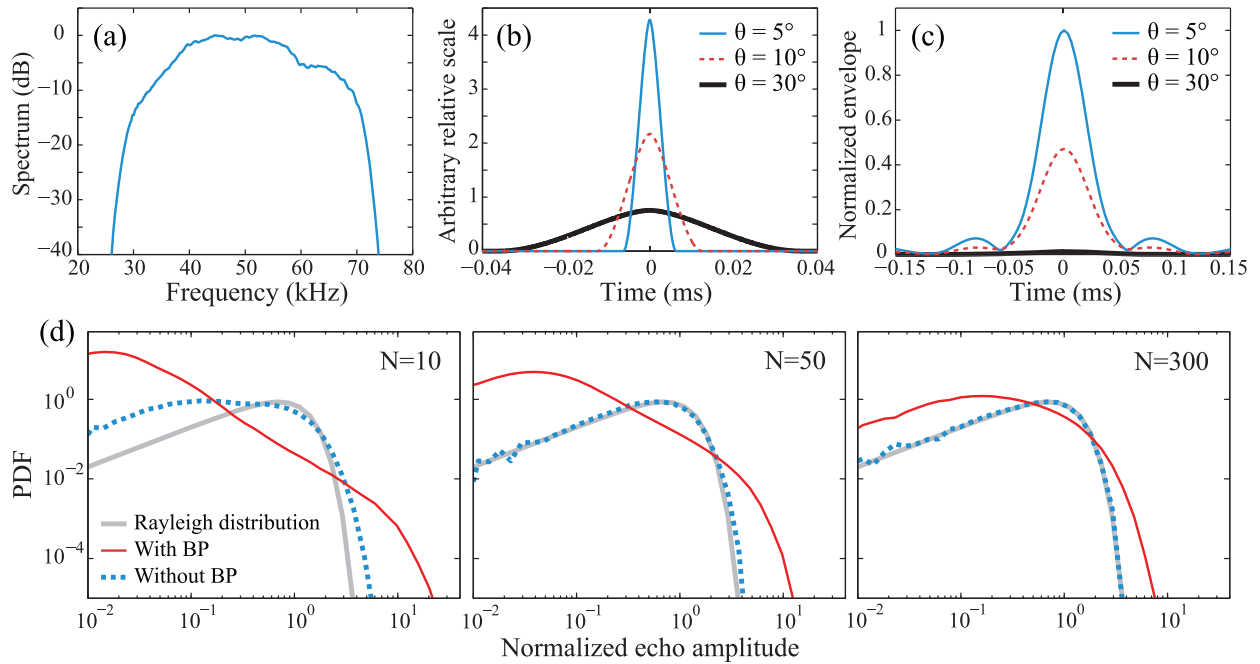


Fig. 2. (a) Spectrum of the replica of system-response-modified transmit signal  $y_s(t)$  (the “transmit replica”). This signal is obtained by convolving the computer-generated transmit signal and the frequency-dependent, two-way responses of the transducer as well as the transmit and receive circuits in the system (see Section II-A). (b) Impulse responses at different polar angles of the two-way beampattern for a circular aperture with a radius of 0.054 m. Both the transmit and receive beampatterns are accounted for in the two-way beampattern. Note there are no sidelobes within or outside the window shown. (c) Envelopes of the cross correlation between the autocorrelation function of the transmit replica  $r_{ss}(t)$  and the (two-way) beampattern impulse responses  $h_{i,BP}(t, \theta_i)$  shown in (b), where  $h_{i,BP}(t, \theta_i)$  is varied for each polar angle. Note the sidelobes are always present regardless of the value of  $\theta$ . (d) Broadband echo pdfs generated with and without the beampattern effects. The models are generated using  $N$  Rayleigh scatterers randomly distributed in the hemispherical half-space, each being statistically independent and with the same mean.

TABLE I

THE  $-3$ -dB BEAMWIDTH AND THE ANGLE AND SOLID ANGLE BETWEEN THE FIRST NULLS OF THE BEAMPATTERN AT THREE DIFFERENT FREQUENCIES. THE BEAMWIDTHS ARE CALCULATED FROM THE  $-3$ -dB TO  $-3$ -dB POINTS ON EITHER SIDE OF THE MAINLOBE OF THE TWO-WAY (COMPOSITE) BEAMPATTERN. THE ANGLES BETWEEN FIRST NULLS ARE CALCULATED FROM THE NULLS ADJACENT TO EITHER SIDE OF THE MAINLOBE. THE SOLID ANGLES ARE SUBTENDED WITHIN THE FIRST NULL ADJACENT TO THE MAINLOBE. SEE APPENDIX A FOR AN ILLUSTRATION OF THESE QUANTITIES

Frequency (kHz)	$-3$ dB beamwidth ( $^\circ$ )	Angle between first nulls ( $^\circ$ )	Solid angle within first null (steradian)
30	19.7	68.8	$0.175 \times 2\pi$
50	11.8	39.6	$0.059 \times 2\pi$
70	8.4	28.0	$0.030 \times 2\pi$

the mainlobe contribute the most to the tail of the echo pdf [6], [16]. The scaling factor relating  $N$  and the number of scatterers in the mainlobe can be determined from the ratio of the solid angle subtended by the null adjacent to the mainlobe and the half-space solid angle (Appendix A).

Unless otherwise noted, the models presented in this study are evaluated using parameters consistent with a high-frequency broadband (30–70 kHz) acoustic transducer used underwater and described in Section III-A. The transducer aperture is circular with a radius of 0.054 m. The  $-3$ -dB beamwidth, the solid angle subtended by the mainlobe, and the number of scatterers within the mainlobe are all frequency dependent (Tables I and II). In this particular application, the signal  $y(t)$  in (1) has a uniform spectrum across frequency based on a rectangular window and the system response  $s(t)$  has nonuniform amplitude across frequency as measured during system calibration [Fig. 2(a)]. Note that the replica used for pulse compression processing of echo data collected by the broadband echosounder system was  $y(t)$  (i.e., without modification from the transducer and circuits in the system), as opposed to the system-response-modified transmit replica  $y_s(t)$  used in the model. However, the

TABLE II

COMPARISON OF THE TOTAL NUMBER OF SCATTERERS WITHIN THE ANALYSIS GATE IN THE HALF-SPACE ( $N$ ) (I.E., INCLUDING MAINLOBE AND ALL SIDELOBES) AND THE AVERAGE NUMBER OF SCATTERERS IN THE ANALYSIS GATE WITHIN THE MAINLOBE OF THE BEAM (I.E., WITHIN THE FIRST NULL) [6]. THE CALCULATION IS BASED ON THE CENTER FREQUENCY (50 kHz) OF THE BROADBAND TRANSDUCER (30–70 kHz) USED IN THE OCEAN EXPERIMENT (SEE SECTIONS II-A AND II-B FOR DETAILS)

$N$ (hemispherical shell in half-space)	Average number within mainlobe at 50 kHz
10	0.59
20	1.18
50	2.96
100	5.91
200	11.83
500	29.57
800	47.31

difference between the replica is inconsequential because, as demonstrated in [19], the  $S_V$  and TS are independent of replica.

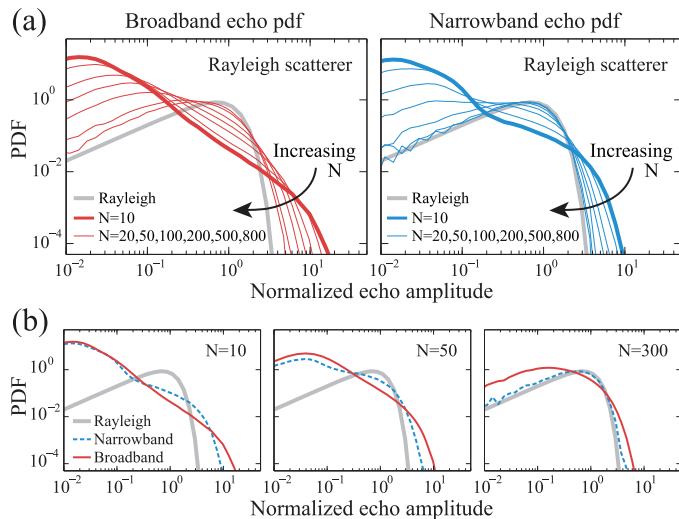


Fig. 3. (a) Model predictions of broadband (left) and narrowband (right) echo pdfs due to monotype aggregations (with beampattern effects). The  $N$  Rayleigh scatterers are randomly distributed in the hemispherical shell, and each is statistically independent and with the same mean value. The shape of the echo pdf varies from highly non-Rayleigh toward the Rayleigh distribution with an increasing number of scatterers in both cases. The narrowband echo pdf is evaluated at the center frequency of the broadband signal (50 kHz). (b) Comparison of the broadband and narrowband echo pdf models from (a) for several examples of fixed  $N$ .

### B. Broadband Beampattern Effects

When randomly located scatterers are observed through a directional beampattern of a transducer, a random amplitude modulation factor is correspondingly imposed on the received echoes due to the random locations in the beam [Fig. 1(a)]. These “beampattern effects” are particularly important in modeling the non-Rayleigh features in the resultant echo pdf [14], [21]. For narrowband signals, this random modulation can be described by a fixed “beampattern pdf,” which can be evaluated numerically using an analytical formula and incorporated in calculating the resultant echo pdf. However, for broadband signals, the modeling is more complex. Since the beampattern of a given transducer is frequency dependent, the beampattern modulation effects for broadband signals are also frequency dependent and vary significantly with increasingly extended tails at higher frequencies (see Appendix B).

In this study, the frequency-dependent beampattern modulation is described by the filtering effects applied through the beampattern impulse response  $h_{i, \text{BP}}(t, \theta_i, \phi_i)$  [Fig. 2(b) and (c)]. Scatterers located near the axis of the transducer aperture are included in the mainlobe of the beampattern at all frequencies, whereas scatterers located farther away from the axis of the aperture are included in the mainlobe at only lower frequencies and fall into the sidelobes at higher frequencies. Therefore, the filtering effects of the broadband beampattern response resemble those of an “all-pass” filter and “lowpass” filter for scatterers located near and farther away from the axis of the transducer aperture, respectively. This location- and frequency-dependent variation explains the observed changes in the beampattern impulse responses [Fig. 2(b)], where the temporal span of the impulse response increases as a function of increasing polar angle ( $\theta_i$  defined in Section II-A). Similar to the narrowband echo pdfs [14, Fig. 4], non-Rayleigh

features are much more pronounced for broadband echo pdfs generated under the influence of beampattern effects when compared with the cases in which the broadband beampattern effects are neglected [Fig. 2(d)].

To illustrate the importance of accounting for the broadband nature of the signals and the associated frequency-dependent beampattern response, broadband and narrowband echo pdfs generated based on the same circular aperture are compared (Fig. 3). Both models are generated using the Rayleigh scatterers that will be described in Section II-C. The narrowband echo pdfs are calculated following the same numerical procedure as in Section II-A, using overlapping sinusoidal waves (narrowband echoes) at 50 kHz. This frequency is chosen to be at the center of the usable band of the modeled broadband (30–70 kHz) transducer. The sinusoidal waves are weighted by the narrowband beampattern response determined by the locations of random scatterers in the beam.

The shape of the broadband echo pdf for a given  $N$  is shown to be significantly more non-Rayleigh (i.e., heavy-tailed) than that of its narrowband counterpart [Fig. 3(b)]. Furthermore, the shape of the broadband echo pdf varies monotonically from non-Rayleigh toward the Rayleigh distribution with increasing  $N$  [Fig. 3(a)]. This latter result is consistent with the prediction made using the narrowband echo pdf models [14] and the intuitive understanding of the Rayleigh distribution as an asymptotic limit of the envelope of the coherent sum of a large number of random scatterers. The pronounced non-Rayleigh features in the broadband echo pdfs are the key to applying echo statistics analysis to acoustic data collected in the ocean.

### C. Models of Scatterer Responses

Three scatterer models are used in this study [through the term  $h_{i, \text{scat}}(t)$  in (4)] to generate broadband echo pdfs (Table III). The first involves scatterers with Rayleigh distributed echo amplitudes before beampattern effects (defined above as “Rayleigh scatterers”). The other two scatterers are both elongated which result in strongly non-Rayleigh echoes before beampattern effects. These include randomly rough, randomly oriented prolate spheroids (hereafter referred to as “prolate spheroid scatterers”) and scatterers modeled as fish swimbladders with realistic length and angle of orientation parameters (hereafter referred to as “fish-like scatterers”). The generic Rayleigh and prolate spheroid scatterers are described in this section, whereas the fish-like scatterers are described in Section IV-A in the context of an application involving acoustic scattering by fish.

Broadband echo pdf models derived using Rayleigh scatterers offer a baseline reference for direct comparison of this model to its narrowband counterpart in previous studies [14], [15] (Fig. 3). The Rayleigh distributed echo amplitudes can be interpreted as either being due to a small (unresolved) compact patch of diffusely distributed scatterers, each with random phase, or being due to a single randomized scatterer whose size, complex internal and/or external structure, angle of orientation, etc., are random and result in many random-phase echoes with random phases from the various features. Overall, the Rayleigh scatterer is a simple first-order approximation to the otherwise more complex scatterers. In spite of its simplicity, it

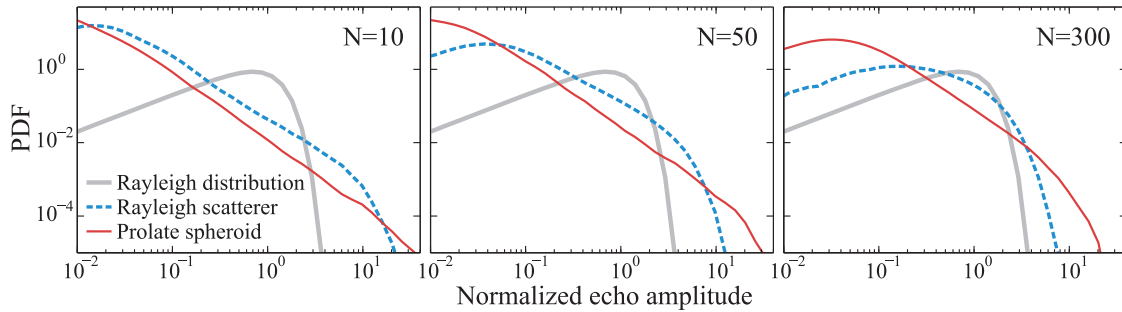


Fig. 4. Model predictions of broadband echo pdfs due to the Rayleigh and prolate spheroid scatterers (with beampattern effects). The prolate spheroid scatterers are of the same length and aspect ratio ( $\xi = 20$ ), and with the angle of orientation uniformly distributed between  $[0, 2\pi)$ . All scatterers are randomly distributed in the hemispherical half-space and statistically independent. The Rayleigh scatterers have the same mean value.

TABLE III  
THE THREE SCATTERER MODELS USED IN THIS STUDY AND THE ASSOCIATED PARAMETERS

Scatterer type	Echo amplitude distribution (before beampattern effects)	Physical description	Frequency dependency	Parameters	Sec.
Rayleigh	Rayleigh	Random phase scatterer or small patch of scatterers [14]	No	All have same mean within monotype aggregation	II.C
Prolate spheroid	Non-Rayleigh	Randomly rough, randomly orientated prolate spheroids [25]	No	Aspect ratio (major/minor axes): $\xi=20$ Single length Orientation distribution: $[0, 2\pi)$	II.C
Fish-like	Non-Rayleigh	Broadband fish backscattering model, swimbladder only [19]	Yes	Swimbladder volume <sup>a</sup> : $V_{00}(25) = 13 \text{ cm}^3$ Length distribution <sup>b</sup> : trawl catches (multiple lengths) Orientation distribution <sup>c</sup> : $[\theta_{\text{mean}}, \theta_{\text{std}}] = [-13^\circ, 10^\circ]$	IV.A

<sup>a</sup> $V_{00}(L_f)$  denotes the equilibrium swimbladder volume of herring at sea surface with a length of  $L_f$  in cm. Following [19], the equilibrium swimbladder volumes of fish of other lengths are calculated by  $V_{00}(L_f) = 0.000808L_f^3 - 0.044264L_f^2 + 0.98075L_f - 7.174827$ .

<sup>b</sup>The length of the swimbladder is  $\frac{1}{3}L_f$  and does not change with depth. The swimbladder volume compresses according to Boyle's law.

<sup>c</sup>The angle of orientation is estimated by fitting a normal distribution with mean  $\theta_{\text{mean}}$  and standard deviation  $\theta_{\text{std}}$  to data reported in [31].

has been useful in describing echoes from naturally occurring objects such as individual wildy moving fish [24]. Note that the Rayleigh-distributed echo amplitudes are assumed to be uniform over the frequency range of interest.

While the Rayleigh scatterer is convenient and describes many scattering geometries, it falls short of describing an important class of scatterer—elongated scatterers that are ubiquitous in nature. The echoes from elongated scatterers, such as when they are randomly oriented, have been shown to be strongly non-Rayleigh [25]. Rough prolate spheroids are a convenient first-order approximation to the shape of elongated scatterers. The echo statistics model of rough prolate spheroids used in this study is based on the analytical solution derived by Bhatia *et al.* [25], where the roughness is introduced heuristically into an analytical backscattering model of an impenetrable smooth prolate spheroid at the high-frequency limit. In this limit, the echo amplitudes are independent of frequency and follow a strongly non-Rayleigh distribution due to the directional scattering of the prolate spheroid [25], [26]. The degree to which the echo amplitude distribution is non-Rayleigh increases with increasing aspect ratio  $\xi$ , where  $\xi$  is defined as the ratio of the major to minor axes of the prolate spheroid.

In this study, the prolate spheroids are assumed to be of the same length and randomly and uniformly distributed across all angles, with  $\xi$  fixed at 20. Combined with the 3-D random locations of the prolate spheroids in the beam and the analysis gate (Section II-A), this is a more general case than that in [25], where the locations and orientations of prolate spheroids are confined to within the plane containing the maximum response axis (MRA) of the transducer.

The broadband echo pdf models computed using the Rayleigh and prolate spheroid scatterers are compared to show the influence of non-Rayleigh features of individual scatterers on the echo pdf of aggregations of scatterers randomly distributed throughout the beam (i.e., mainlobe and all sidelobes) (Fig. 4). Calculations are made with broadband beampattern effects [see Fig. 2(d) for the effects with and without the beampattern with Rayleigh scatterers; Bhatia *et al.* [25] show the effects with and without the beampattern with prolate spheroids]. All pdfs are non-Rayleigh with significant differences in the tails. For a given  $N$ , the degree to which the tail is elevated (and, hence, the echo pdf is non-Rayleigh) is greater with the prolate spheroid scatterers.

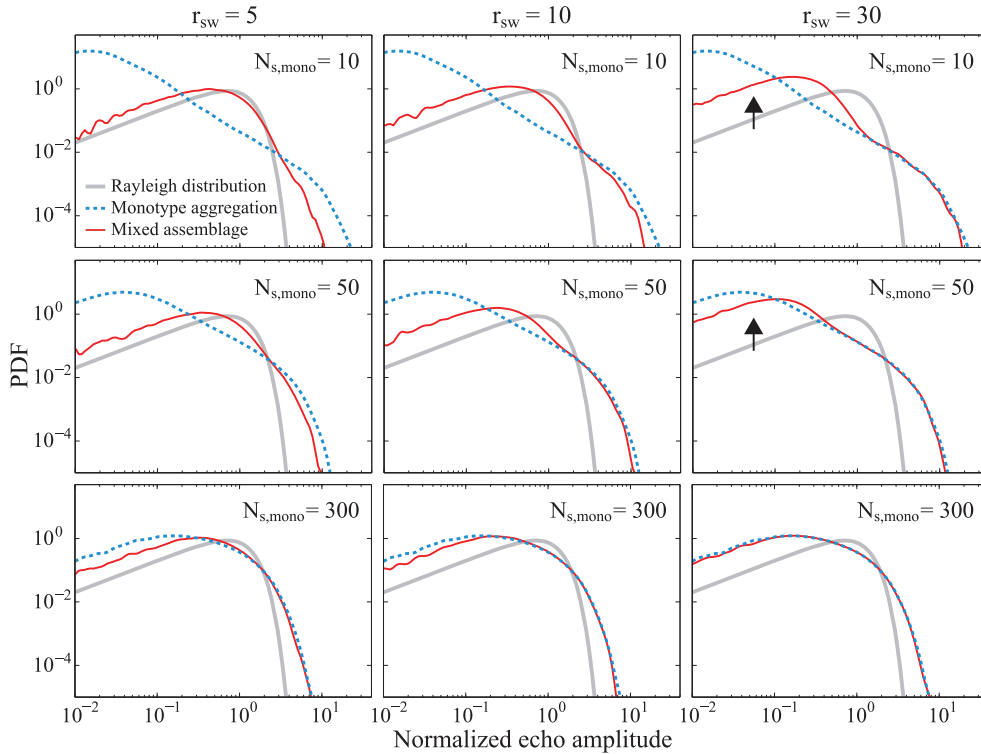


Fig. 5. Model predictions of broadband echo pdfs (with beampattern effects) for both monotype aggregations and mixed assemblages of scatterers randomly distributed in the hemispherical shell. The mixed assemblages are composed of two types of scatterers of different scattering amplitudes. The ratio of the ensemble-averaged backscattering cross section of the strong to weak scatterers in the mixed assemblages ( $r_{sw}$ ) and the number of strong or monotype scatterers in the analysis gate ( $N_{s,mono}$ ) are both varied.  $N_{s,mono}$  is equal to the total number of scatterers and the number of strong scatterers in monotype aggregations and mixed assemblages, respectively. The number of weak scatterers in the mixed assemblages is fixed at 1000. Rayleigh scatterers are used in all predictions with each being statistically independent. The scatterers in the monotype aggregations have the same mean value.

#### D. Broadband Echo PDFs From Mixed Assemblages of Scatterers

In this section, broadband echo pdf models associated with mixed aggregations of scatterers in the analysis window are investigated. In all analyses above, the broadband echo pdf models are evaluated for “monotype aggregations” while varying the number of identical types of scatterers ( $N$ ) in the analysis window (Figs. 3 and 4). However, in nature, “mixed assemblages” are also common, where there is more than one type of scatterer spatially interspersed and uniformly distributed in the analysis window [15]. Here, the same “type” of scatterers refers to scatterers with the same scattering amplitude distribution and mean scattering amplitude [15]. Rayleigh scatterers are used here in order to simplify interpretation of the modeling results.

Broadband echo pdf models are formulated for mixed assemblages composed of two types of scatterers with varying combinations of the numbers of the strong and weak scatterers ( $N_s$  and  $N_w$ , respectively) and different ratios of the ensemble-averaged backscattering cross section of the strong to the weak scatterers ( $r_{sw}$ ) (see [15, eq. (3)]). Broadband echo pdfs from monotype aggregations and mixed assemblages are compared in cases with varying numbers of scatterers  $N_{s,mono}$ , where  $N_{s,mono} = N$  for monotype aggregations, and  $N_{s,mono} = N_s$  for mixed assemblages (Fig. 5). When  $r_{sw}$  is small, the overall shapes of broadband echo pdfs for mixed assemblages and monotype aggregations are distinctly different. When  $r_{sw}$  is large, the strong scatterers dominate the scattering field, and the shapes of the

broadband echo pdfs only differ in the low echo amplitude portion (indicated by arrows in Fig. 5). As expected, the shape of the broadband echo pdf approaches the Rayleigh distribution with increasing numbers of scatterers in both cases.

### III. EXPERIMENTAL DATA FROM THE OCEAN

#### A. Acoustic Data Collection and System Calibration

Acoustic echo data were collected using a towed broadband echosounder (EdgeTech) during a series of fish backscattering experiments over Georges Bank in the Gulf of Maine in September 2008. The acoustic measurements were accompanied by a pelagic rope trawl deployed by a separate vessel. The net catches provided important ground truth information on the species composition of the observed fish aggregations as well as the length distribution of each fish species. Details of the experiments and the broadband echosounder system are given in [27] and [19], respectively.

This study used data collected from three broadband channels in the echosounder system with usable frequency bands spanning 1–6, 10–18, and 30–70 kHz. Data from all three channels were used to measure the broadband  $S_V$  encompassing the resonance of the fish swimbladder at the lowest frequencies to the geometric scattering regime at the higher frequencies. As discussed in Section II-A, the replica used in pulse compression processing is  $y(t)$ . The echo statistics analysis was limited to data from the 30–70-kHz channel. This channel was chosen for its broad bandwidth and consequently better temporal resolution after pulse compression processing, based on

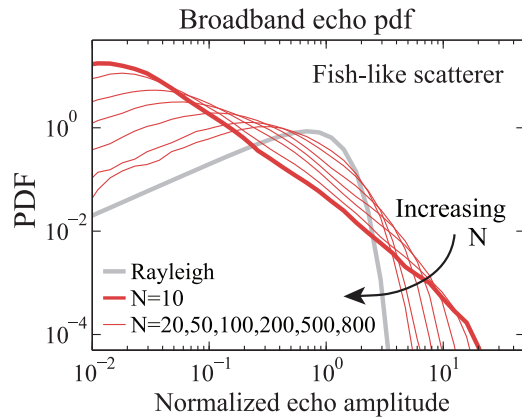


Fig. 6. Broadband echo pdfs (with beampattern effects) calculated using the fish-like scatterers with prescribed random distributions of length and angle of orientation as discussed in Section IV-A. The  $N$  fish are randomly distributed in the hemispherical shell and are statistically independent of each other.

which non-Rayleigh echo pdfs are more likely to be observed. This channel was also chosen because it contains one of the operational frequencies, 38 kHz, widely used in fisheries studies. The echosounder system was calibrated using the partial-wave approach described in [28] and the calibration was corroborated with results from conventional full-wave calibration procedure [29].

### B. Selection of Acoustic Data for Echo Analysis

Several factors are accounted for in selecting data for the analysis of numerical density of fish based on both the echo statistics and  $S_V$  (echo energy). To simplify the inference and comparison, aggregations containing fish of similar size and the same species are selected. Data that are strongly non-Rayleigh are chosen so that statistical inferences could be made using the model developed in this paper (see Section IV and Fig. 6 for details). Inference is conducted for data extracted from analysis windows within fish aggregations where the composition appears homogeneous. Details of the data selection are given below.

1) *Calculating Broadband Echo PDF and  $S_V$  From Data:* Echo data are selected based on features in the broadband echo pdf and  $S_V$  associated with fish aggregations observed through the use of echograms [Fig. 7(a)]. Echograms are maps of depth versus horizontal distance color coded by the magnitudes of echo envelope time series after pulse compression (using the equations given in Section II-A). The depth is inferred by the two-way travel time between the source and the along-range echo sample. The horizontal distance is calculated based on the echosounder pinging interval and its towed speed measured concurrently. These echograms are of similar nature to those produced using narrowband echo envelopes.

The broadband echo pdf and  $S_V$  are calculated using data enclosed by analysis windows in the echogram [Fig. 7(a)]. Specifically, each broadband echo pdf is estimated through the kernel density method (as described in Section II-A) using all echo envelope samples in the analysis window normalized to the root mean square magnitude of the ensemble. Broadband  $S_V$  is estimated using the same set of data enclosed in the analysis window via the multitaper method, which reduces spectral estimation bias by averaging multiple independent estimates of the

spectrum through orthogonal data tapers [30]. The time-half-bandwidth parameter is set at 30, which results in a frequency concentration of a few kilohertz for the associated Slepian tapers.

2) *Selection of Fish Aggregations:* To simplify the inference and comparison using both echo statistics and  $S_V$  (echo energy) for estimating the numerical density of fish, monospecific aggregations of Atlantic herring (*Clupea harengus*) are identified through a combination of the observed resonance of swimbladder near 3.7 kHz [Fig. 7(b)], prior knowledge of the survey region, and trawl catches. This fish is the dominant species in the local piscifauna of the survey region. By constraining the analysis to monospecific, and thus, monotype aggregations (Section II-D), and using the distributions of fish length and angle of orientation from trawl catches [27] and previous studies [31], respectively, the number of unknown parameters in the inference is minimized.

Another key element of the analysis is selecting fish aggregations that cause strongly non-Rayleigh echoes to allow echo statistics analysis [Fig. 7(c)]. Due to the spreading of the sonar beam, for a fixed numerical density of fish, there will be a smaller number of fish within an analysis gate at a closer range than in a gate of the same duration at a larger range. Echoes (after pulse compression) from a smaller number of scatterers tend to only partially overlap and are more non-Rayleigh. Therefore, fish observed at the closer ranges will tend to cause non-Rayleigh echoes.

Based on the above criteria, inference of the numerical density of fish is focused on monospecific herring aggregations that occurred near the seafloor in early morning (approximately two hours after first light) [Fig. 7(a)]. The selected aggregations were at a range of approximately 40 m from the towed broadband echosounder system. The pitch and roll angles of the broadband echosounder system were relatively constant during these periods, as the system towed at the deep depth was not strongly influenced by the ship motion at surface. This minimizes fluctuations in the echoes caused by towbody-induced changes in the overall range and angle of orientation of fish with respect to the echosounder, which creates an advantageous condition for echo statistics analysis.

3) *Selection of Analysis Windows:* Two important considerations for selecting analysis windows for the inference study are the independence between echo samples and the stationarity of the scattering processes from which the echoes originate. Due to the inherently patchy spatial structure of organism aggregations in the sea, this results in two competing criteria: 1) the analysis window needs to be sufficiently large to include enough independent echo samples to form a representative ensemble for inferences based on echo statistics; and 2) the analysis window needs to be sufficiently small so that the scattering processes, such as those associated with the composition and numerical density of fish in this study, within the window are stationary. Analysis windows are chosen from the interior of monospecific herring aggregations (those identified in Section III-B2) where the echogram appears visually homogeneous over color scale variations as large as 10 dB. The analysis windows span 5–8 pings and over a depth range of 3–6 m, which includes 529–1057 along-range complex (analytic) echo samples

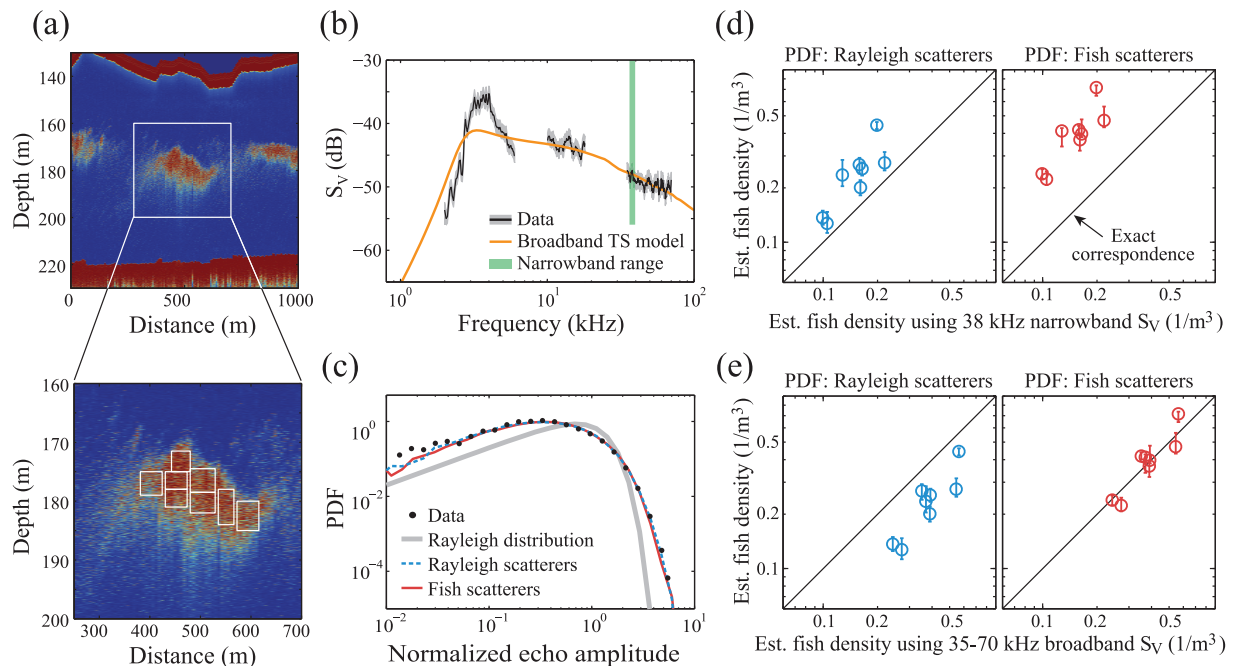


Fig. 7. Data analysis procedure and estimates of the numerical density of monospecific herring aggregations observed near the seafloor during day time. (a) Echogram of the selected herring aggregation and the analysis windows. The white boxes in the lower panel indicate the analysis windows from which the numerical densities of fish in (d) and (e) are estimated. (b) Observed broadband volume backscattering strength ( $S_V$ ) and the best fitting broadband TS model. Also shown is the range of frequency (36.3–39.7 kHz; centered at 38 kHz) included to calculating the narrowband  $S_V$ . Empirical measurements of the distributions of the angle of orientation and fish length are used to constrain the parameters of the broadband TS model (see Section IV-A). Since the broadband TS model is inherently inaccurate near the resonance region of the fish swimbladder, a different model was used to infer the swimbladder volume from the  $S_V$  data at resonance (also see Section IV-A for details). (c) Broadband echo pdf of the data and the best fitting broadband echo pdf model predictions using both the Rayleigh and fish-like scatterers. Predictions using each type of scatterer achieved a good fit to the data, although requiring different numerical densities. (d) Comparison of the numerical density of fish estimated using the broadband echo pdf model based on the Rayleigh and fish-like scatterers and the narrowband TS model. (e) Comparison of the numerical density of fish estimated using the broadband echo pdf model based on the Rayleigh and fish-like scatterers and the *broadband* TS model.

in the 30–70-kHz channel sampled at 130.2 kHz (data decimated through the use of analytic signal). This results in typically several thousand echo samples in the analysis windows.

The echo samples enclosed in the analysis windows are generally independent due to the geometry of the scatterers and the echosounder. Given the combination of the narrow beam pattern, ping rate of one per 4 s, the tow speed of the echosounder at approximately 3 kn, and the distance from the echosounder to the scatterers, echo samples from adjacent pings are likely from a different set of scatterers as they are separated by distances greater than the footprint of the mainlobe of the sonar beam. The fish aggregations are characterized by strong non-Rayleigh echoes, which indicate that long-range echoes (after pulse compression) within the same ping likely originate from different resolved scatterers whose echoes only partially overlap with phases randomly and uniformly distributed over  $[0, 2\pi)$ . While some adjacent echo envelope samples within the same ping may not be statistically independent when the numerical density of scatterer is high (i.e., the time series is oversampled), estimation of the echo pdf is still possible provided that enough independent samples are included in the ensemble.

Stationarity is implicitly assumed for the composition of the fish aggregation within the analysis windows to allow the use of all enclosed echo samples for the inference. Specifically, ping-to-ping variations in the echoes are assumed to have been produced solely by changes in the angles of orientation of the scatterers with respect to the echosounder and their random locations in the sonar beam. The numerical density, mean scattering

amplitude, as well as the distribution of scattering amplitude of the fish insonified over consecutive pings in the same analysis window are also assumed identical. Formal statistical analysis on stationarity is outside the scope of this study but may be attempted using methods such as those used in [32].

#### IV. ESTIMATION OF THE NUMERICAL DENSITY OF FISH IN MONOSPECIFIC HERRING AGGREGATIONS

In this section, the broadband echo pdf formulation is used as an inference tool to estimate the numerical density of fish from selected monospecific herring aggregations described above in Section III. The formulation is applied using two models of individual scatterers, assuming the fish to be 1) Rayleigh scatterers (as described in Section II-C) and 2) fish-like scatterers (as described in detail in Section IV-A). Results of the statistics-based density estimates are compared with densities estimated using conventional echo energy techniques and TS models. This comparison is important as echo energy has been traditionally used in this field to infer absolute fish density. It is especially important in this study as absolute fish density was not obtainable with the nets used. The goal of this comparison is to assess the applicability and performance of the broadband echo pdf model in analyzing real-world data collected from the ocean.

##### A. Broadband Fish Backscattering Model

The fish backscattering model used here was derived from physics principles and thus inherently broadband [19]. Different

from the model in [19] which combined the predicted backscattering contributions from the fish swimbladder and flesh incoherently (i.e., summation of backscattering cross sections), the contribution of fish flesh is not included here. This is because 1) the backscattering contribution from fish flesh is negligible compared to that of the swimbladder in this study; and 2) a complex backscattering amplitude is needed to generate random echo amplitude samples for the broadband echo pdf model, which prevents the use of the incoherently combined backscattering cross section in [19]. The scattering from the fish swimbladder is predicted using the deformed cylinder formulation [33], which accounts for both the size and shape of the organ. The shape of the swimbladder is modeled using the circular cross-sectional profiles of a prolate spheroid but with its centerline adjusted to achieve a flat dorsal surface [29]. This shape bears a greater resemblance to the typical shape of a herring swimbladder [34] than the regular prolate spheroidal shape used in [19]. The longitudinal axis of the fish swimbladder is assumed to be parallel to the longitudinal axis of the fish (i.e., the swimbladder is not tilted within the fish). All other model parameters remain unchanged from those used in [19]. In contrast to the cases with the Rayleigh and prolate spheroid scatterers, frequency-dependent variations in the backscattering amplitude resulting from changes in the angle of orientation and length of fish are incorporated in this model and used to generate broadband echo pdf models [through the term  $h_{i,\text{scat}}(t)$  in (4)].

Parameters of the fish backscattering model are determined by a combination of empirical data and theoretical modeling (Table III). The angle of orientation of the fish with respect to the echosounder is generated independently by drawing random samples from a normal distribution derived from data reported in [31] (see  $[\theta_{\text{mean}}, \theta_{\text{std}}]$  in Table III). Since the empirical angles are relative to the horizontal plane, the scattering predictions are constrained to using angles that vary only in the MRA plane (Section II-C), causing errors for predictions of scattering by fish out of that plane. However, echoes that dominate the tail of the echo pdfs are from fish near the MRA, making this a reasonable approximation for the narrowbeam echosounder used.

The fish length is determined by drawing random samples from the distribution of fish length derived from trawl catches [27, Fig. 4(c)]. The length of the swimbladder is fixed at 1/3 of the fish length for all depths, whereas the width of the swimbladder is calculated using the swimbladder volume as compressed by the depth of the fish. To estimate the compressed swimbladder volume, an equilibrium swimbladder volume ( $V_{00}$ ) of a 25-cm herring at the sea surface is first inferred by matching the predicted resonance frequency of a gas-filled prolate spheroid (with a volume compressed from  $V_{00}$  to the depth of the fish) and the observed resonance frequency of the fish swimbladder [Fig. 7(b)]. The resonance frequency of a gas-filled prolate spheroid is predicted using a modified version of Ye's model [35] that includes both viscosity and thermal damping in addition to radiation damping. The compressed swimbladder volume of fish of other lengths at depth are then estimated by scaling the equilibrium swimbladder volume according to an empirical third-order polynomial relationship (Table III) and compressing the volume by Boyle's law.

Using the above parameters, broadband echo pdfs are calculated for a range of number of fish  $N$  in the hemispherical shell. The shapes of the echo pdfs vary from being highly non-Rayleigh toward the Rayleigh distribution as a function of increasing  $N$  (Fig. 6). This trend is consistent with those of the Rayleigh and prolate spheroid scatterers (Figs. 3 and 4).

### B. Method for Estimating Density Using Echo Statistics

Broadband echo pdfs are computed using the Rayleigh and fish-like scatterers over a range of numbers of scatterers in the analysis gate ( $N = 100\text{--}3000$  at a spacing of 100) and used to estimate the numerical density of fish from the statistics of echo data. The numerical density of scatterers associated with a given echo pdf model is

$$\rho_{\text{stat}} \approx \frac{N}{(2\pi r^2 L_g)} \quad (6)$$

where  $r$  is the distance between the center of the analysis window and the echosounder, and the term in the parentheses represents the volume enclosed by the hemispherical shell in Fig. 1(a). A maximum likelihood estimator (MLE) is used to select the echo pdf model that best fits the data. The value of  $N$  from the best fit model is then used to calculate the density in (6).

Assume  $x_1, x_2, \dots, x_m$  are  $m$  independent and identically distributed echo samples included in the analysis window, the MLE computes the log-likelihood

$$\begin{aligned} \ell(N|x_1, x_2, \dots, x_m) &= \ln p_{\text{model}}(x_1, x_2, \dots, x_m|N) \\ &= \ln \prod_i^m p_{\text{model}}(x_i|N) \\ &= \sum_i^m \ln p_{\text{model}}(x_i|N) \end{aligned} \quad (7)$$

where  $p_{\text{model}}(x_i|N)$  is the likelihood of observing echo envelope amplitude  $x_i$  given  $N$  scatterers in the analysis gate  $L_g$ . The MLE performs inference by maximizing the log-likelihood function

$$\hat{N}_{\text{MLE}} = \arg \max_N \ell(N|x_1, x_2, \dots, x_m).$$

The confidence interval of the estimation can be determined using

$$\left\{ \rho : 2 \left( \ell \left( \hat{N}_{\text{MLE}} \right) - \ell(N) \right) < c_\alpha \right\} \quad (8)$$

where  $c_\alpha$  is the  $(1 - \alpha)$ -level quantile of the  $\chi_k^2$  distribution and  $k$  is equal to the dimension of the parameter space ( $k = 1$  in this study) [36]. The confidence intervals are used to plot the error bars in Fig. 7(d) and (e). Since the echo pdf models are computed only for a limited number of values of  $N$ , only discrete samples of  $\ell(N)$  can be calculated based on the data. Therefore, a cubic-spline interpolation is used to obtain a smooth log-likelihood function for estimating the best fit and the confidence interval.

The above formulation of MLE requires all samples  $x_1, x_2, \dots, x_m$  to be independent. This may be violated despite the various criteria taken in Section III-B to select the fish

aggregation and analysis windows. However, information required to formulate the MLE using conditional probabilities of dependent samples is difficult to obtain for the current data set. Intuitively, adjacent correlated samples are not as informative as independent samples. Therefore, the current assumption may lead to underestimation of the confidence intervals if the samples are dependent.

### C. Methods for Estimating Density Using Echo Energy

The numerical density of fish is also estimated using echo energy techniques based on the measured  $S_V$  and TS models. A narrowband semi-empirical TS model and a broadband physics-based TS model are used here. These estimates provide independent references with which the estimates given by the echo statistics methods can be compared.

The narrowband semi-empirical TS model (hereafter referred to as the “narrowband TS model”) was derived by Ona using a regression analysis of *in situ* TS measured from herring using 38-kHz narrowband echosounders [37]. This model accounts for the depth-dependent compression of the fish swimbladder as well as the variation contributed by fish of different lengths. The distribution of fish length is obtained from samples collected with our trawl [27, Fig. 4(c)].

The narrowband volume backscattering strength  $\overline{S_{V,NB}}$  is calculated by averaging the broadband  $S_V$  measurement across a frequency band centered at 38 kHz with a bandwidth of 3.4 kHz [36.3–39.7 kHz, marked by the vertical shading in Fig. 7(b)], consistent with those of the echosounder systems used in [37]. The overbar  $\overline{\cdot}$  denotes the operation of calculating the average value on a linear scale (i.e., backscattering cross section for TS and backscattering coefficient for  $S_V$ ). It is also an industry standard in fisheries management to estimate the numerical density of fish using narrowband echosounders at 38 kHz based on empirical or semi-empirical models [38]. The predicted narrowband TS ( $\overline{TS_{NB}}$ ) is averaged on a linear scale over the distribution of fish length and used to estimate the numerical density of fish using

$$\rho_{NB} = 10^{(\overline{S_{V,NB}} - \overline{TS_{NB}})/10}. \quad (9)$$

The broadband physics-based TS model (hereafter referred to as the “broadband TS model”) uses the same fish backscattering model and parameters as with the fish-like scatterers for the broadband echo pdf model (see Section IV-A). The predicted broadband TS ( $TS_{BB}$ ) is averaged on a linear scale over the distributions of fish length and angle of orientation and used to estimate the numerical density of fish using

$$\rho_{BB} = 10^{(\overline{S_{V,BB}} - TS_{BB})/10} \quad (10)$$

where  $S_{V,BB}$  is the observed broadband backscattering strength in the 30–70-kHz channel. Note the fish density is estimated using the averaged difference between the predicted broadband TS and the observed volume backscattering strength over 30–70 kHz.

Note for both the narrowband and broadband TS cases, the confidence interval of the backscattering strength given by the multitaper method is used directly as an approximation of the confidence interval of the estimated numerical density of fish.

Exact estimation of the confidence interval in the presence of nuisance parameters (such as  $\theta_{\text{mean}}$ ,  $\theta_{\text{std}}$ , and  $V_{00}$  in this study) is beyond the scope of this study.

### D. Comparing Statistics and Energy Model Estimates of Numerical Density of Fish

The numerical density of fish estimated using the echo statistics and echo energy techniques are compared [Fig. 7(d) and (e)]. In general, the trends with which the fish density estimates vary are consistent for all models and all analysis windows in the selected aggregation. Specifically, the symbols in Fig. 7(d) and (e) are roughly parallel to the line of exact correspondence for all models and sample windows. Fish densities estimated using the narrowband TS model are lower than the corresponding estimates given by both the broadband TS model [by comparing the  $x$  values across Fig. 7(d) and (e)] and the broadband echo pdf model, for the cases with either the Rayleigh or fish-like scatterers [Fig. 7(d)]. In contrast, fish densities estimated using broadband echo pdf model with fish-like scatterers show good correspondence with estimates given by the broadband TS model [Fig. 7(e)]. These two methods make use of the same baseline broadband fish backscattering model (Section IV-A) and the same data set (acoustic measurements collected on the 30–70-kHz channel), but with fundamentally different bases of inference (echo statistics versus echo energy).

### E. Discussion

Fish densities estimated using all three models follow the same trend in each analysis window within an aggregation [Fig. 7(d) and (e)]. In addition, when using the fish-like scattering model, fish densities estimated using the broadband echo pdf model are in good agreement with fish densities estimated using the broadband TS model. This analysis shows that, when used as an inference tool, the broadband echo pdf model can achieve a similar level of performance as with the conventional echo energy methods. Since the echo pdf method involves normalizing the data (hence removing calibration as a factor), it has the advantage of not requiring absolute calibration of the system. However, the assessment of the different models based on absolute fish density estimates is limited due to the lack of ground truth information on the actual numerical density of fish—an issue that is common to many fisheries studies. Each model is also subject to constraints and biases resulting from the model assumptions and choices of model parameters. These considerations are discussed below.

1) *Potential Sources of Errors for Echo Energy Methods:* The discrepancy between fish density estimates given by the narrowband TS model with those given by the other two models may be explained by the semi-empirical nature of this model. Although fish density estimation based on 38-kHz narrowband measurements is the industry standard in fisheries management, the application of semi-empirical or empirical models is only justified when the distribution of angle of orientation and general behavior of the observed aggregation is similar to the aggregations based on which the model is derived. Therefore, extrapolating the narrowband TS model derived using measurements from Norwegian herring to the acoustic data collected in a distant geographical location (Gulf of Maine in this study) is likely

to introduce errors. The quantification of such errors is difficult and requires careful selection of comparable experimental data collected from the ocean.

The results also show the importance of incorporating broadband information on the estimation of fish density using echo energy methods. Specifically, fish densities estimated by the broadband TS model are consistently higher than fish densities estimated by the narrowband TS model, despite the overlap in acoustic frequency of the data used. The narrowband estimates can be erroneous due to the issues of extrapolation as discussed above, whereas the broadband estimates can easily be influenced by the choice of model parameters, including  $V_{00}$ ,  $\theta_{\text{mean}}$ , and  $\theta_{\text{std}}$  (Section IV-A). By allowing these model parameters to vary, a separate investigation using a similar broadband TS model that fit the full broadband data from all three broadband channels (1–6, 10–18, and 30–70 kHz) produced fish density estimates that are intermediate between the narrowband estimates and the current high-frequency-only (30–70 kHz) broadband estimates (not shown).

Results of the analyses expose the problem of model extrapolation for empirical or semi-empirical models and illustrate the challenges associated with physics-based models in terms of model sensitivity to the exact choice of model parameters, which include the shape and volume of swimbladder, as well as the distributions of the length and angle of orientation of fish in this study.

2) *Influence of the Model of Individual Scatterers on the Broadband Echo PDF Model:* The choice of the model of individual scatterers is crucial for modeling the broadband echo pdfs. With a fixed number of scatterers in the analysis gate, the shape of the modeled echo pdf (with beampattern effects) is more non-Rayleigh when using individual resolved scatterers with more non-Rayleigh echo features before beampattern effects (Fig. 4). Consequently, fish densities estimated based on echo pdf models generated using non-Rayleigh scatterers (such as the fish-like scatterers) are higher than those estimated based on echo pdfs generated using the Rayleigh scatterers [Fig. 7(d) and (e)]. Since the Rayleigh distribution is the asymptotic limit of the statistical features of echoes from complex sources [24], [26], scatterer densities estimated based on echo pdf models generated using the Rayleigh scatterers can be viewed as a lower bound to the true density.

Broadband echo pdf models generated using fish-like scatterers with wider angle of orientation distributions are also observed to be more non-Rayleigh compared to those generated using narrower angle of orientation distributions (not shown). This can be understood intuitively by considering the scattering beampattern of elongated scatterers, where its sidelobes produce analogous effects as the receiving beampattern modulation induced by the sidelobes of the receiver [25]. A wider angle of orientation distribution includes a higher number of sidelobes and therefore will produce echo pdfs that are more non-Rayleigh. In this study, the distribution of the angles of orientation of fish is modeled using a distribution derived from data reported for herring in Norwegian waters [31]. Quantification of the associated errors is difficult due to the lack of information on the angle of orientation distribution of herring in the study region.

The shapes of the broadband echo pdf models generated using the prolate spheroid scatterers are more non-Rayleigh than the pdf models generated using the fish-like scatterer (compare Figs. 4 and 6). This is due to differences in both the angle of orientation distribution of the scatterers and the associated frequency-dependent echo response. Specifically, the angle of orientation and length of the fish-like scatterers follow the prescribed distributions discussed in Section IV-A, whereas the prolate spheroid scatterers are of the same length and oriented uniformly between  $[0, 2\pi)$ . Furthermore, despite their similar baseline prolate spheroidal shapes (Section IV-A) and matching aspect ratios ( $\xi = 20$ ), only the fish-like scatterers contain the realistic frequency-dependent echo amplitude variation induced by varying orientations. Similar to the significance of including the frequency-dependent broadband beampattern effects [Figs. 2(d) and 3], this result further emphasizes the importance of incorporating frequency-dependent information in modeling broadband echo pdfs.

3) *Other Modeling Considerations for the Broadband Echo PDF Model:* The broadband echo pdf model is evaluated assuming that the scatterers are randomly and uniformly distributed in the entire space enclosed by the hemispherical shell between the analysis gate [Fig. 1(a)]. However, fish aggregations in the ocean tend to occur in horizontal layers with a limited vertical span and do not fill the space as the scatterers in the model. Therefore, echoes collected in field experiments are more likely to originate from scatterers located within or near the mainlobe of the sonar beam as well as in adjacent sidelobes. This effectively reduces the degree to which the resulting echo pdf is non-Rayleigh when the same number of scatterers is included in the analysis gate. Therefore, the current model may overestimate the numerical density of scatterers in the observed aggregations.

Furthermore, the influence of noise is not accounted for in this study. The inclusion of noise will make the echo pdf model tend toward the Rayleigh distribution [39]. Therefore, inference made based on the noise-free models will tend to overestimate the numerical density of scatterers in the observed aggregations. However, since the signal-to-noise ratio of the echo data in the 30–70-kHz channel is generally above 20 dB in this study (not shown), the impact of noise on the estimation results is likely negligible.

## V. SUMMARY AND CONCLUSION

In this study, a physics-based numerical model is developed to predict the pdf of the magnitude of complex broadband echoes for sonar/radar systems. The broadband echo pdfs contain heavy tails and are significantly more non-Rayleigh than their narrowband counterparts (Fig. 3). This is because broadband pulse-compressed echoes will generally only partially overlap for low to medium density of scatterers, as opposed to the heavily overlapping sinusoidal waves in the narrowband case. The modeling results further show the significance of incorporating the broadband frequency-dependent characteristics of the system, signal, scatterers, and the beampattern modulation effects of the sonar/radar receiver in modeling the non-Rayleigh statistical features of broadband echoes. The

non-Rayleigh shape of the broadband echo pdf provides the discriminative features that are key to the application of echo statistics methods in analyzing experimental data and assessing system performance.

The broadband echo pdf model is applied successfully to acoustic data collected from ocean experiments. The model is implemented using parameters that are from the broadband (30–70 kHz) echosounder used. The variation of the shape of the broadband echo pdfs from highly non-Rayleigh toward the Rayleigh distribution as a function of increasing numerical density of scatterers is used as an inference tool to estimate the numerical density of fish in the observed monospecific herring aggregations (Fig. 7). The fish densities estimated using the broadband echo pdf model follow the same trend as the fish densities independently estimated using echo energy techniques. The comparisons greatly improve when the bandwidth of the models and measurements are matched, as well as when using a realistic (fish-like) scattering model. Specifically, the comparison is best when the fish densities estimated using the broadband echo pdf model are compared with the density estimates given by a broadband physics-based TS model and broadband echo energy data from the 30–70-kHz band, with both models using fish-like (elongated) scatterers. While the analysis is limited by the lack of ground truth of the numerical density of fish—a common issue with many fisheries studies—these results establish the first-order applicability of echo statistics methods to broadband acoustic data collected in the field. In addition, as with narrowband echo statistics methods developed in the past, this approach has the advantage over echo energy methods as it does not require absolute calibration of the system, and bypasses the uncertainty associated with spectral estimation of echoes.

The analysis shows the importance of the model of individual scatterers in modeling the broadband echo pdf. It is demonstrated that non-Rayleigh features in the echoes of individual resolved scatterers (before beampattern effects) contribute significantly to non-Rayleigh features in the echoes from aggregations of these individual scatterers (with beampattern effects) (Fig. 4). Given the prevalence of elongated, and thus non-Rayleigh, scatterers in nature [25], [26], incorporating realistic non-Rayleigh features of individual scatterers is critical to the application of echo statistics methods to real-world data. In addition, a lower bound to the estimated numerical density of scatterers can be achieved by using broadband echo pdf models generated based on modeled scatterers with Rayleigh-distributed envelope magnitudes.

The analysis also exposes the challenges associated with the large number of free parameters in inference problems in fisheries acoustics. For example, in this study, a broadband physics-based backscattering model for fish is used both for generating the fish-like scatterers in the broadband echo pdf model and predicting the broadband TS of fish for use with echo energy techniques (Section IV-A). The prediction of backscattering from this broadband physics-based model can be sensitive to the choice of model parameters, such as the shape and volume of the swimbladder, as well as the distributions of the length and angle of orientation of the fish. In fact, in the inference for the numerical density of the fish, these free model

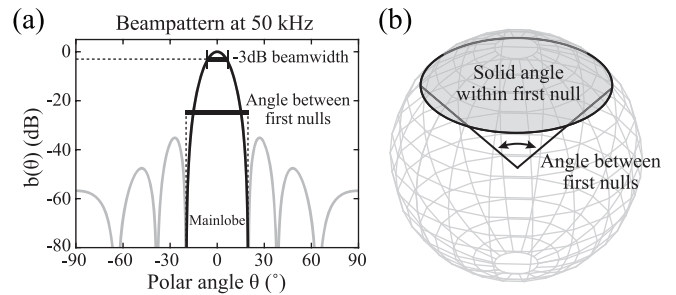


Fig. 8. (a) The two-way beampattern at 50 kHz and the definition of  $-3$ -dB beamwidth and the angle between first nulls. (b) An illustration of the solid angle subtended by the angle between the first nulls.

parameters are nuisance parameters that have to be taken into account for the inference to be conducted. In combination with the continuing efforts to enhance the quality of ground truth information using net, optical, and acoustical imaging methods [40]–[42], the Bayesian inference framework may provide an avenue to systematically incorporate prior knowledge of the survey region and investigate the effects of these model parameters in future studies [43].

The development of the broadband echo pdf model is motivated in the context of acoustic scattering studies of marine organisms, and the model is applied in this study to analyze broadband echoes of fish collected in ocean experiments. However, the model is formulated based on principles of physics and signal processing and can be applied to analyze broadband echoes collected in different environments using different systems, such as radar. Since the application of echo statistics methods does not require absolute calibration of the system, the analysis can be implemented rapidly during field experiments to obtain a rough estimation of the target(s) of interest before detailed analyses are conducted. As a tool to characterize the statistical features of the echoes, the broadband echo pdf model provides an additional dimension of information complementary to the temporal and spectral features of the echoes that form the basis toward more accurate interpretation of broadband echo data.

## APPENDIX A

### BEAMWIDTH AND SOLID ANGLE SUBTENDED BY MAINLOBE

The beamwidth of a given transducer aperture is often characterized by its  $-3$ -dB beamwidth, which is the angle between the  $-3$ -dB points on either side of the mainlobe [Fig. 8(a)]. In this study, the angle between the first nulls on either side of the mainlobe [Fig. 8(a)] is also identified to calculate the solid angle subtended by the mainlobe of the two-way (composite) beampattern [Fig. 8(b)]. For a given polar angle  $\theta$ , the solid angle subtended by  $\theta$  around the axis of the transducer aperture is  $2\pi(1 - \cos\theta)$ . The half-space solid angle is  $2\pi$ .

## APPENDIX B

### BEAMPATTERN EFFECTS

The echo amplitude observed by a sonar/radar receiver is modulated by the two-way beampattern depending on the locations of the scatterers in the beam. For randomly located scatterers, the statistical distribution corresponding to the random

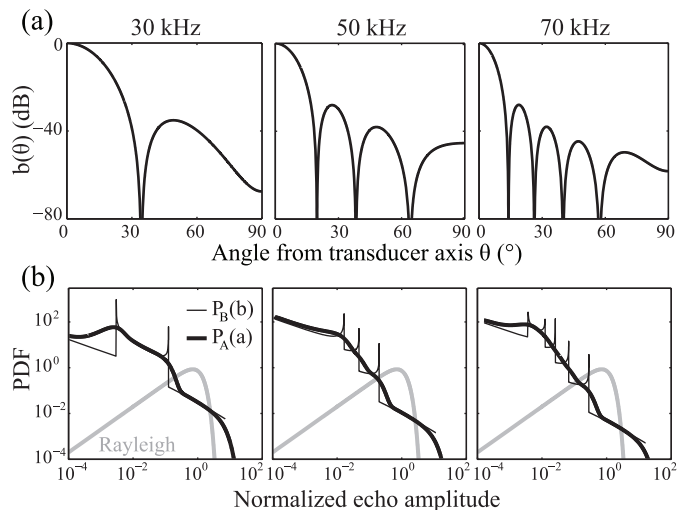


Fig. 9. (a) Narrowband beampatterns of a circular aperture with a radius of 0.054 m calculated at 30, 50, and 70 kHz, corresponding to  $-3$ -dB to  $-3$ -dB two-way beamwidths of  $19.7^\circ$ ,  $11.8^\circ$ , and  $8.4^\circ$ , respectively. (b) The beam pattern pdf  $p_B(b)$  and the associated echo pdf  $p_A(a)$  (after beam pattern effects) resulting from observing a single Rayleigh scatterer randomly located in the beam (hemispherical half-space).

weighting factor associated with the beam is termed the “beam pattern pdf”  $p_B(b)$ , which can be derived analytically using the beam pattern of the transducer  $b(\theta)$  [14], [21]. Such “beam pattern effects” are frequency dependent and are illustrated here using three examples of narrowband echo pdfs calculated assuming a circular aperture with a radius of 0.054 m (Fig. 9). The pdfs are calculated with three beam patterns whose mainlobes have  $-3$ -dB to  $-3$ -dB two-way beamwidths of  $19.7^\circ$ ,  $11.8^\circ$ , and  $8.4^\circ$ , corresponding to the range of frequencies (30–70 kHz) used in the ocean experiment. A single Rayleigh scatterer is used in each example. The term  $p_A(a)$  is the pdf of the echo amplitude after beam pattern effects. The tail of the echo pdf is shown to vary monotonically and further extended with increasing frequency.

#### ACKNOWLEDGMENT

The authors would like to thank Dr. A. Lavery, Dr. J. Preisig, and Dr. A. Solow at the Woods Hole Oceanographic Institution (WHOI) for their thoughtful suggestions.

#### REFERENCES

- [1] “Special Issue on Non-Rayleigh Reverberation and Clutter,” *IEEE J. Ocean. Eng.*, vol. 35, no. 2, pp. 233–356, Apr. 2010.
- [2] “Special Issue on Radar Clutter,” *IET Radar Sonar Navig.*, vol. 4, no. 2, pp. 143–328, 2010.
- [3] T. K. Stanton and C. Clay, “Sonar echo statistics as a remote-sensing tool: Volume and seafloor,” *IEEE J. Ocean. Eng.*, vol. OE-11, no. 1, pp. 79–96, Jan. 1986.
- [4] D. A. Abraham and A. P. Lyons, “Novel physical interpretations of  $K$ -distributed reverberation,” *IEEE J. Ocean. Eng.*, vol. 27, no. 4, pp. 800–813, Oct. 2002.
- [5] T. K. Stanton, “Density estimates of biological sound scatterers using sonar echo peak PDFs,” *J. Acoust. Soc. Amer.*, vol. 78, no. 5, pp. 1868–1873, 1985.
- [6] T. K. Stanton, D. Chu, J. M. Gelb, G. L. Tipple, and K. Baik, “Interpreting echo statistics of three distinct clutter classes measured with a midfrequency active sonar: Accounting for number of scatterers, scattering statistics, and beam pattern effects,” *IEEE J. Ocean. Eng.*, vol. 40, no. 3, pp. 657–665, Jul. 2015.

- [7] J. W. Goodman, *Statistical Optics*, 1st ed. New York, NY, USA: Wiley-Interscience, 1985, sec. 2.9.
- [8] N. P. Chotiros, “Non-Rayleigh distributions in underwater acoustic reverberation in a patchy environment,” *IEEE J. Ocean. Eng.*, vol. 35, no. 2, pp. 236–241, Apr. 2010.
- [9] T. C. Gallaudet and C. P. de Moustier, “High-frequency volume and boundary acoustic backscatter fluctuations in shallow water,” *J. Acoust. Soc. Amer.*, vol. 114, no. 2, pp. 707–725, 2003.
- [10] J. M. Gelb, R. E. Heath, and G. L. Tipple, “Statistics of distinct clutter classes in midfrequency active sonar,” *IEEE J. Ocean. Eng.*, vol. 35, no. 2, pp. 220–229, Apr. 2010.
- [11] P. A. Crowther, “Fluctuation statistics of sea-bed acoustic backscatter,” in *Bottom-Interacting Ocean Acoustics*. Boston, MA, USA: Plenum, 1981, pp. 609–622.
- [12] D. A. Abraham and A. P. Lyons, “Reverberation envelope statistics and their dependence on sonar bandwidth and scattering patch size,” *IEEE J. Ocean. Eng.*, vol. 29, no. 1, pp. 126–137, Jan. 2004.
- [13] A. P. Lyons, S. F. Johnson, D. A. Abraham, and E. Pouliquen, “High-frequency scattered envelope statistics of patchy seafloors,” *IEEE J. Ocean. Eng.*, vol. 34, no. 4, pp. 451–458, Oct. 2009.
- [14] D. Chu and T. K. Stanton, “Statistics of echoes from a directional sonar beam insonifying finite numbers of single scatterers and patches of scatterers,” *IEEE J. Ocean. Eng.*, vol. 35, no. 2, pp. 267–277, Apr. 2010.
- [15] W.-J. Lee and T. K. Stanton, “Statistics of echoes from mixed assemblages of scatterers with different scattering amplitudes and numerical densities,” *IEEE J. Ocean. Eng.*, vol. 39, no. 4, pp. 740–754, Oct. 2014.
- [16] B. A. Jones, J. A. Colosi, and T. K. Stanton, “Echo statistics of individual and aggregations of scatterers in the water column of a random, oceanic waveguide,” *J. Acoust. Soc. Amer.*, vol. 136, no. 1, pp. 90–108, 2014.
- [17] K. G. Foote *et al.*, “Measuring the frequency response function of a seven octave bandwidth echo sounder,” *Proc. Inst. Acoust.*, vol. 21, no. 1, pp. 88–95, 1999.
- [18] A. C. Lavery, D. Chu, and J. N. Moum, “Measurements of acoustic scattering from zooplankton and oceanic microstructure using a broadband echosounder,” *ICES J. Mar. Sci.*, vol. 67, no. 2, pp. 379–394, 2010.
- [19] T. K. Stanton, D. Chu, J. M. Jech, and J. D. Irish, “New broadband methods for resonance classification and high-resolution imagery of fish with swimbladders using a modified commercial broadband echosounder,” *ICES J. Mar. Sci.*, vol. 67, no. 2, pp. 365–378, 2010.
- [20] D. Chu and T. K. Stanton, “Application of pulse compression techniques to broadband acoustic scattering by live individual zooplankton,” *J. Acoust. Soc. Amer.*, vol. 104, no. 1, pp. 39–55, 1998.
- [21] J. Ehrenberg, “A method for extracting the fish target strength distribution from acoustic echoes,” in *Proc. IEEE Conf. Eng. Ocean Environ.*, 1972, pp. 61–64.
- [22] D. W. Scott, *Multivariate Density Estimation: Theory, Practice, and Visualization*. New York, NY, USA: Wiley, 1992, ch. 6.
- [23] Z. I. Botev, J. F. Grotowski, and D. P. Kroese, “Kernel density estimation via diffusion,” *Ann. Stat.*, vol. 38, no. 5, pp. 2916–2957, 2010.
- [24] C. S. Clay and B. G. Heist, “Acoustic scattering by fish-acoustic models and a two-parameter fit,” *J. Acoust. Soc. Amer.*, vol. 75, no. 4, pp. 1077–1083, 1984.
- [25] S. Bhatia, T. K. Stanton, and K. Baik, “Non-Rayleigh scattering by a randomly oriented elongated scatterer randomly located in a beam,” *IEEE J. Ocean. Eng.*, vol. 40, no. 1, pp. 169–176, Jan. 2015.
- [26] T. K. Stanton, D. Chu, and D. B. Reeder, “Non-Rayleigh acoustic scattering characteristics of individual fish and zooplankton,” *IEEE J. Ocean. Eng.*, vol. 29, no. 2, pp. 260–268, Apr. 2004.
- [27] T. K. Stanton, C. J. Sellers, and J. M. Jech, “Resonance classification of mixed assemblages of fish with swimbladders using a modified commercial broadband acoustic echosounder at 1–6 kHz,” *Can. J. Fish. Aquat. Sci.*, vol. 69, no. 5, pp. 854–868, 2012.
- [28] T. K. Stanton and D. Chu, “Calibration of broadband active acoustic systems using a single standard spherical target,” *J. Acoust. Soc. Amer.*, vol. 124, no. 1, pp. 128–136, 2008.
- [29] W.-J. Lee, “Broadband and statistical characterization of echoes from random scatterers: Application to acoustic scattering by marine organisms,” Ph.D. dissertation, MIT/WHOI Joint Program, Cambridge/Woods Hole, MA, USA, 2013.
- [30] D. J. Thomson, “Spectrum estimation and harmonic analysis,” *Proc. IEEE*, vol. 70, no. 9, pp. 1055–1096, Sep. 1982.
- [31] I. Huse and E. Ona, “Tilt angle distribution and swimming speed of overwintering Norwegian spring spawning herring,” *ICES J. Mar. Sci.*, vol. 53, no. 5, pp. 863–873, 1996.

- [32] P. Borgnat, P. Flandrin, P. Honeine, C. Richard, and J. Xiao, "Testing stationarity with surrogates: A time-frequency approach," *IEEE Trans. Signal Process.*, vol. 58, no. 7, pp. 3459–3470, Jul. 2010.
- [33] T. K. Stanton, "Sound scattering by cylinders of finite length. III. Deformed cylinders," *J. Acoust. Soc. Amer.*, vol. 86, no. 2, pp. 691–705, 1989.
- [34] S. M. M. Fässler, P. G. Fernandes, S. I. K. Semple, and S. Brierley, "Depth-dependent swimbladder compression in herring *Clupea harengus* observed using magnetic resonance imaging," *J. Fish Biol.*, vol. 74, no. 1, pp. 296–303, 2009.
- [35] Z. Ye, "Low-frequency acoustic scattering by gas-filled prolate spheroids in liquids," *J. Acoust. Soc. Amer.*, vol. 101, pp. 1945–1952, 1997.
- [36] A. Azzalini, *Statistical Inference Based on the Likelihood*. London, U.K.: Chapman & Hall/CRC Press, 1996, vol. 68, ch. 3.
- [37] E. Ona, "An expanded target-strength relationship for herring," *ICES J. Mar. Sci.*, vol. 60, no. 3, pp. 493–499, 2003.
- [38] J. M. Jech, K. G. Foote, D. Chu, and L. C. Hufnagle, "Comparing two 38-kHz scientific echosounders," *ICES J. Mar. Sci.*, vol. 62, no. 6, pp. 1168–1179, 2005.
- [39] T. K. Stanton and D. Chu, "Non-Rayleigh echoes from resolved individuals and patches of resonant fish at 2–4 kHz," *IEEE J. Ocean. Eng.*, vol. 35, no. 2, pp. 152–163, Apr. 2010.
- [40] E. Belcher, W. Hanot, and J. Burch, "Dual-frequency identification sonar (DIDSON)," in *Proc. Int. Symp. Underwater Technol.*, 2002, pp. 187–192.
- [41] P. H. Wiebe and M. C. Benfield, "From the Hensen net toward four-dimensional biological oceanography," *Prog. Oceanogr.*, vol. 56, no. 1, pp. 7–136, 2003.
- [42] C. S. Davis *et al.*, "A three-axis fast-tow digital video plankton recorder for rapid surveys of plankton taxa and hydrography," *Limnol. Oceanogr., Methods*, vol. 3, no. 2, pp. 59–74, 2005.
- [43] S. M. M. Fässler, A. S. Brierley, and P. G. Fernandes, "A Bayesian approach to estimating target strength," *ICES J. Mar. Sci.*, vol. 66, no. 6, pp. 1197–1204, 2009.



**Wu-Jung Lee** received the B.S. degree with a double major in electrical engineering and life science (with zoology focus) at the National Taiwan University, Taipei City, Taiwan, in 2005 and the Ph.D. degree in acoustical oceanography from the Massachusetts Institute of Technology/Woods Hole Oceanographic Institute (MIT/WHOI) Joint Program in Applied Ocean Science and Engineering, Boston/Woods Hole, MA, USA, in 2013. Her doctoral research focused on broadband and statistical characterization of random scatterers, inspired in the context of

acoustic scattering by marine organisms observed through artificial sonar systems.

She is currently a Postdoctoral Fellow in the Department of Psychological and Brain Sciences, Johns Hopkins University, Baltimore, MD, USA, working on the biological sonar systems of bats and toothed whales. She was the F.V. Hunt Postdoctoral Research Fellow of the Acoustical Society of America from 2014 to 2015. Her research involves the measurement and modeling of echolocation signals and prey echoes toward understanding the neural computation for auditory scene analysis and sensorimotor integration for active biological sonar systems.



**Timothy K. Stanton** received the B.S. degree from Oakland University, Rochester, MI, USA, in 1974 and the M.S. and Ph.D. degrees from Brown University, Providence, RI, USA, in 1977 and 1978, respectively, all in physics. His undergraduate research involved experiments in solid-state acoustics with Dr. N. Tepley as advisor and his graduate research involved nonlinear acoustics measurements and instrumentation development with Dr. R. Beyer as advisor.

From 1978 to 1980, he was a Senior Engineer with the Submarine Signal Division, Raytheon Company, Portsmouth, RI, USA, where he was engaged in research, development, and testing of acoustic systems. From 1980 to 1988, he was a Member of the Scientific Staff, Department of Geology and Geophysics, University of Wisconsin, Madison, WI, USA, where he conducted various theoretical, laboratory, and field studies in acoustical oceanography with Dr. C. Clay. From 1988 to the present, he has been a Member of the Scientific Staff, Department of Applied Ocean Physics and Engineering, Woods Hole Oceanographic Institution (WHOI), Woods Hole, MA, USA. From 1997 to 2001, he was Chair of the Department and currently is a Scientist Emeritus. He is collaborating with colleagues in the development of models of acoustic scattering by marine organisms through various theoretical and laboratory methods, physics-based models of the statistics of scattered signals, and is applying the methods to ocean measurements. In addition to his research, he is part of the Massachusetts Institute of Technology (MIT), Cambridge, MA, USA and WHOI Joint Graduate Education Program and teaches acoustic scattering theory. Overall he has published papers covering the areas of nonlinear acoustics, acoustics instrumentation, fiber-optic hydrophones, echo statistics, and acoustic scattering by volumetric objects, seafloor, sea surface, and the underside of sea ice.

Dr. Stanton has served as an Associate Editor for the *Journal of the Acoustical Society of America* and as a Guest Editor for a special issue of *Deep Sea Research*. He has also served as a Guest Editor for a special issue of the *IEEE JOURNAL OF OCEANIC ENGINEERING*. He is a Fellow of the Acoustical Society of America and a Member of The Oceanography Society. In 1985, he was awarded the A.B. Wood medal for Distinguished Contributions to Underwater Acoustics. He held the Adams Chair at WHOI from 2011 to 2015.